Electrochemically Self-Driven Integration of FeSe/FeS Heterostructures for Enhanced Sodium Storage and Rapid Kinetics

Hui Li[a], Yanchen Fan[b], Guangshuai Han[c], Xin Zhang[a], Haoxi Ben[d], Claire (Hui) Xiong[*e], Chunrong Ma[*df], Zhaoying Li[*a]

[a] Power Engineering Major, School of Mechanical and Electrical Engineering, Qingdao University, Qingdao 266071, China

[b] PetroChina Shenzhen New Energy Research Institute, Shenzhen, 518000, China

[c] School of Automotive Studies, Tongji University, Shanghai 201804, China

[d] Laboratory of Bio-Fibers and Eco-Textiles, Qingdao University, Qingdao 266071, China

[e] Micron School of Materials Science and Engineering, Boise State University, Boise, ID 83725, United States

[f] College of Textiles & Clothing, Qingdao University, Qingdao 266071, China; Key

*E-mail: clairexiong@boisestate.edu (corresponding author)

zhaoyli@qdu.edu.cn

Experimental section

Material synthesis

The composite was synthesized by sol-gel method. To be specific, First, 1.5 g Sodium alginate (SA) were added to 80 mL deionized water under vigorous stirring for at least 3 h form solution A. In the meantime, 20 mg of graphene oxide (GO) were also dissolved in 20 mL of deionized water by ultrasonic treatment to obtained solution B.

Thereafter, solution B was injected quickly into solution A and stirred for 30 min. Then the mixed solution was injected to the solution of $Fe(NO_3)_3$ solution dropwise. The prepared aerogel particles were frozen with nitrogen and freeze-dry. Subsequently, the dried particles and selenium powder and sulfur powder in a 1:5:5 mass ratio were loaded at each end of a quartz boat and then calcined at 600 ◦C under Ar/H_2 atmosphere for 2 h to obtain the $FeSe_{0.8}S_{0.2}$-SC composite. For comparison, the FeSe sample is synthesized similarly, but FeSe-C synthesized without adding sulfur powder.

"The material was synthesized no unexpected or unusually high safety hazards were encountered"

Material characterization

The crystal phases of the as-synthesized materials were recorded by X-ray diffraction (XRD, Rigaku, Cu Ka radiation). Field emission scanning electron microscopy (FESEM, JEOL JSM-7800F) and energy dispersive spectroscopy (EDS, OXFORD X-Max) and transmission electron microscopy (TEM, JEM 2100F, 200 kV) were fulfilled to obtain the structure and morphology of all samples. The electronic states of all samples were tested using X-ray photoelectron spectroscopy performed on an ESCALAB Xi^+ electron spectrometer (Thermo Fisher Scientific, US), employing 300 W Al Kα radiation. The situations of free radicles were reflected by electron paramagnetic resonance (EPR) conducted under vacuum on a Bruker A300 instrument. During the initial charge/discharge cycle, the phase change of the sample was determined using *In situ* XRD spectroscopy. The examination of ^{23}Na magic-angle-spinning (MAS) NMR was conducted using a Bruker Avance III spectrometer, operating within a 14.1 T magnetic field and a ^{23}Na Larmor frequency of 132.34 MHz.

Electrochemical measurements

The electrochemical performance of the $FeSe_{0.8}S_{0.2}$-SC and pure FeSe-C anodes were evaluated by assembling 2032-type coin-cells. The working electrode slurry was prepared by blending active materials (80 wt%), Super P (10 wt%), sodium carboxymethylcellulose (10 wt%), and solvent (deionized water). The slurry was evenly pasted on Cu foil and completely dried in a vacuum at 90 °C. The slurry was uniformly spread onto Cu foil and thoroughly dried under vacuum conditions at 90 ℃ for 10 hours. Moreover, the average mass loading of the active materials ranged from 0.6 to 1.2 mg cm^{-2}. The electrolytes were 1 M $NaPF_6$ in ethylene glycol dimethyl ether (DME) for the half cells (with metallic Na as the counter electrode). Whatman GF/D glass fibers were selected for the separators. The cells were assembled within a glove box containing highly pure argon gas (with O_2 and H_2O levels below 0.01 ppm). Galvanostatic charge/discharge profiles were conducted using a LAND-CT3002A battery testing system within a voltage range of 0.01-3 V (vs Na^+/Na). Additionally, cyclic voltammetry (CV) tests were carried out at various scan rates using an electrochemical workstation (CHI650E).

Computational Method

Density Functional Theory (DFT) calculations were executed using periodic super-cells within the framework of the generalized gradient approximation (GGA) and employed the Perdew-Burke-Ernzerhof (PBE) functional for exchange-correlation, along with ultrasoft pseudopotentials for representing nuclei and core electrons. The Kohn-Sham orbitals were described by a plane-wave basis set, with kinetic and charge-density energy cutoffs set to 30 Ry and 300 Ry, respectively. The adsorption energy (ΔE_a) was computed using the equation:

$$\Delta E_a = E_{tot} - E_{Na} - E_{str} \quad \text{(Equation S1)}$$

where E represents the total energy obtained from DFT calculations, Ena is the energy of sodium atoms, and E_{str} denotes the energy of the structure. The charge density difference ($\Delta\rho$) was determined using the equation:

$\Delta\rho=\rho_{AB}-\rho_{A}-\rho_{B}$ (Equation S2)

where AB refers to the combined system, A is the base, and B is the adsorbate. In the computation of the latter two quantities, atomic positions were kept fixed as they appear in the AB system. Fermi-surface effects were managed using the smearing method of Methfessel and Paxton, with a smearing parameter of 0.02 Ry. Brillouin zones were sampled at the Gamma point, and a 3 × 3 × 1 supercell with a vacuum layer of approximately 15 Å was used to negate slab interactions in the z direction. The diffusion barrier for Na atoms was evaluated using the nudged elastic band (NEB) method. All DFT calculations were carried out utilizing the PW and NEB modules of the Quantum ESPRESSO package.

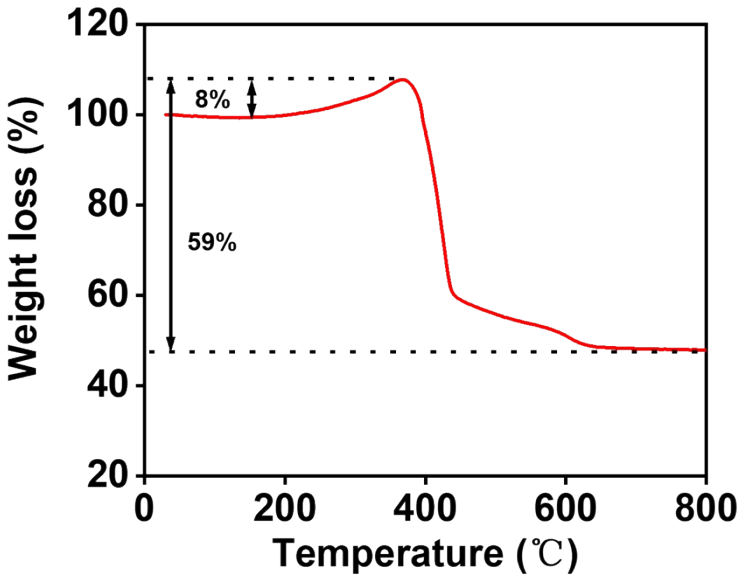

Figure S1 TGA curves of $FeSe_{0.8}S_{0.2}$-SC.

The carbon content in $FeSe_{0.8}S_{0.2}$-SC was 26% (Figure S1).

Based on the mass equation:

$10FeSe_{0.8}S_{0.2}+28O_2 \rightarrow 10Fe_2O_3+5SO_2+8SeO_2+5CO_2$

Assuming the initial mass of the sample is $m_{initial}$, the mass increases by 8%, resulting in $1.08 \times m_{initial}$

After the reaction, the final mass is 48.2% of the increased mass: $1.08 \times m_{initial} \times 0.518$

The mass loss can be calculated as: $m_{loss}=1.08 \times m_{initial} \times 0.482$

According to the reaction, the generation of 5 moles of CO_2 corresponds to 5 moles of C. Therefore, the mass of carbon can be expressed as:

$C=（m_C/m_{loss}）\times 100\% \approx 26\%$

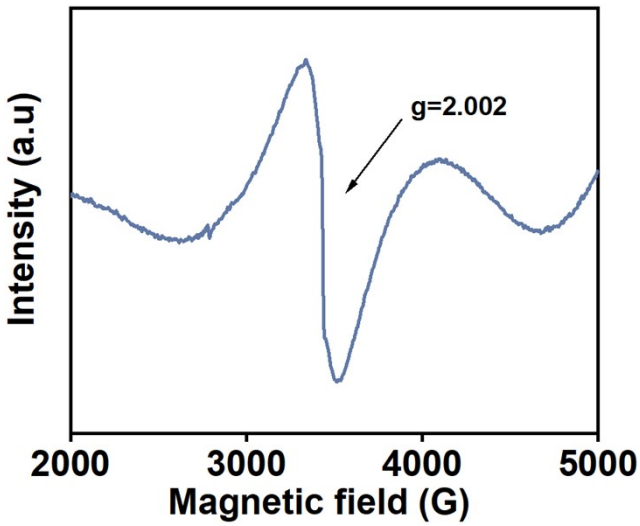

Figure S2 Electron paramagnetic resonance (EPR) of $FeSe_{0.8}S_{0.2}$-SC.

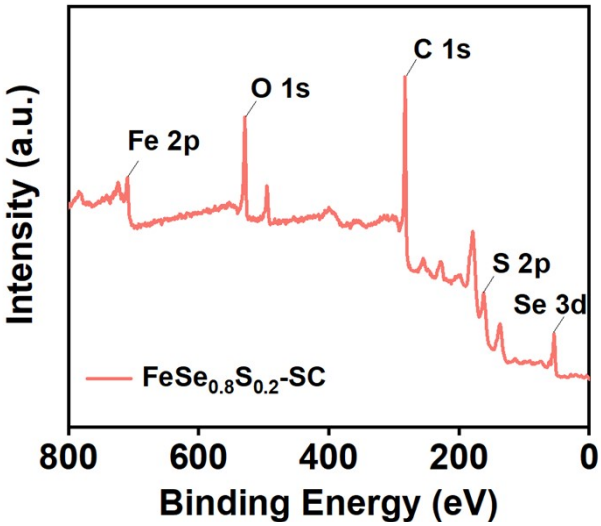

Figure S3 Full XPS spectrum of $FeSe_{0.8}S_{0.2}$-SC.

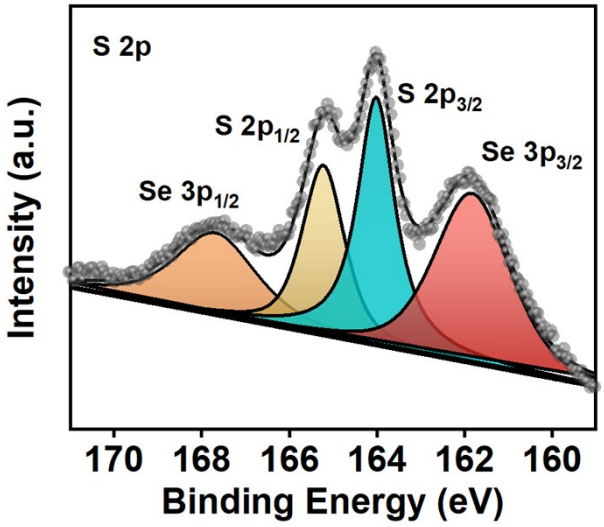

Figure S4 XPS spectra of S 2p of $FeSe_{0.8}S_{0.2}$-SC.

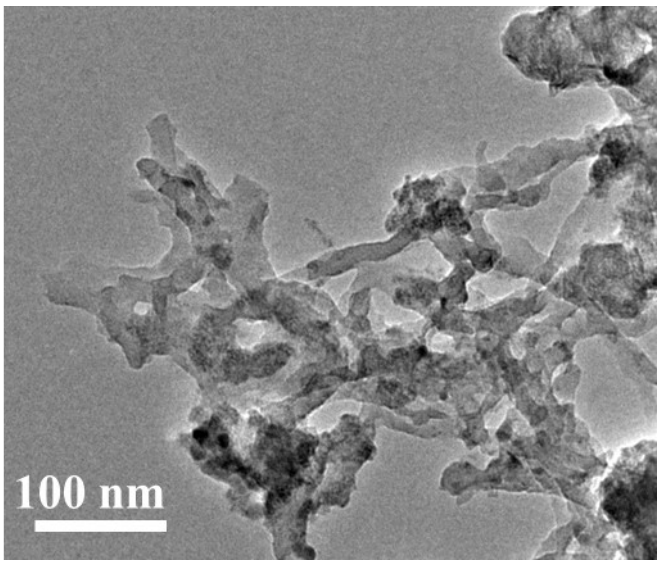

Figure. S5 TEM of the FeSe/FeS-SC sample after cycling.

Table S1 Comparison of cycle and rate performance of FeSe/FeS-SC with previously reported relevant anode materials.

Materials	Specific capacity mAh g^{-1}	Cycling performance	References
$FeSe_{0.8}S_{0.2}$@NC	421 mAh g^{-1} (15 A g^{-1})	3000 cycles (3 A g^{-1})	Our work
Fe_7Se_8@C	167 mAh g^{-1} (8 A g^{-1})	720 cycles (2 A g^{-1})	1
FeS/C	469 mAh g^{-1} (5 A g^{-1})	600 cycles (1 A g^{-1})	2
ZnS@C	267.5 mAh g^{-1} (10 A g^{-1})	550 cycles (1 A g^{-1})	3
Fe_7S_8@S/N-C	347 mAh g^{-1}(1 A g^{-1})	150 cycles (1 A g^{-1})	4
V_2O_5/Ni_3S_2	175 mAh g^{-1} (2 A g^{-1})	600 cycles (0.5 A g^{-1})	5
MoS_2/Sb_2S_3@C	408.7 mAh g^{-1} (10 A g^{-1})	650 cycles (5 A g^{-1})	6
V_5S_8@C	153 mAh g^{-1}(10 A g^{-1})	1000 cycles (2 A g^{-1})	7

1 J. Yuan, Y. Gan, X. Xu, M. Mu, H. He, X. Li, X. Zhang and J. Liu, *J. Colloid Interface Sci.*, 2022, **626**, 355-363.
2 X. Huang, Q. He, J. Xun, T. Pan, S. Zhou, G. Cao and A. Pan, *Sci. China Mater.*, 2023, **66**, 2601-2612.
3 Q. Cu, C. Shang, L. Hu, G. Zhou and X. Wang, *Appl. Surf. Sci.*, 2022, **579**.
4 X. Li, T. Liu, Y. X. Wang, S. L. Chou, X. Xu, A. Cao and L. Chen, *J. Power Sources*, 2020, **451**, 227790.
5 X. Wang, B. Shi, X. Wang, J. Gao, C. Zhang, Z. Yang and H. Xie, *J. Mater. Chem. A*, 2017, **5**, 23543-23549.
6 D. Wang, L. Cao, D. Luo, R. Gao, H. Li, D. Wang, G. Sun, Z. Zhao, N. Li, Y. Zhang, F. Du, M. Feng and Z. Chen, *Nano Energy*, 2021, **87**.
7 L. Li, W. Zhang, X. Wang, S. Zhang, Y. Liu, M. Li, G. Zhu, Y. Zheng, Q. Zhang, T. Zhou, W. K. Pang, W. Luo, Z. Guo and J. Yang, *ACS Nano*, 2019, **13**, 7939-7948.

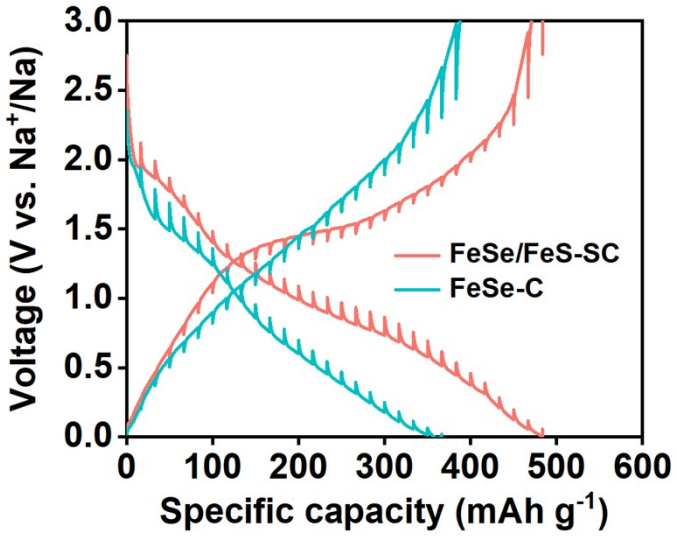

Figure S6 GITT curves of FeSe/FeS-SC and FeSe-C.

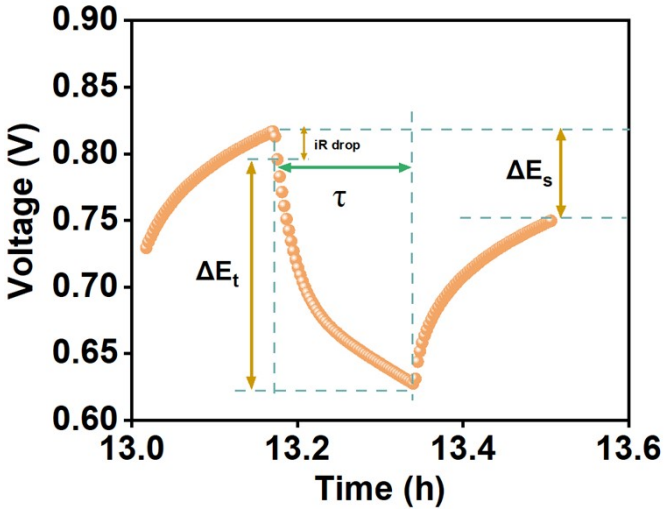

Figure S7 Voltage response over time during a single current pulse.

Figure S7 displayed the voltage response over time during a single current pulse of FeSe/FeS-SC. The D_{Na^+} values can be evaluated by the formula as follow:

$$D_{Na^+} = \frac{4}{\pi\tau}\left(\frac{m_B V_M}{M_b S}\right)^2\left(\frac{\Delta E_s}{\Delta E_t}\right)^2$$

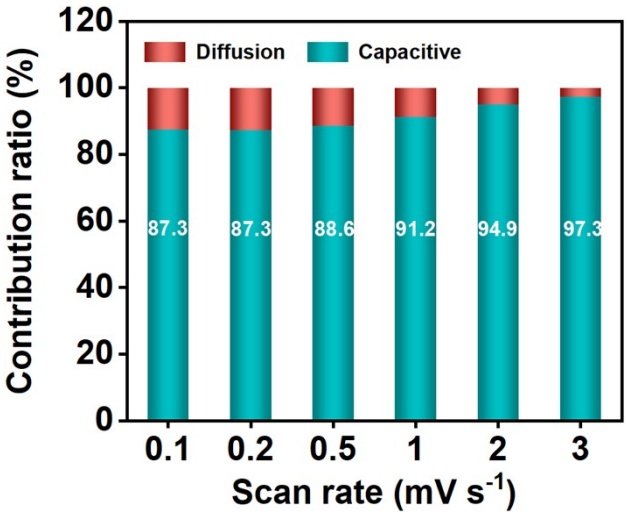

Figure S8 Capacitive contribution ratios of FeSe/FeS-SC.

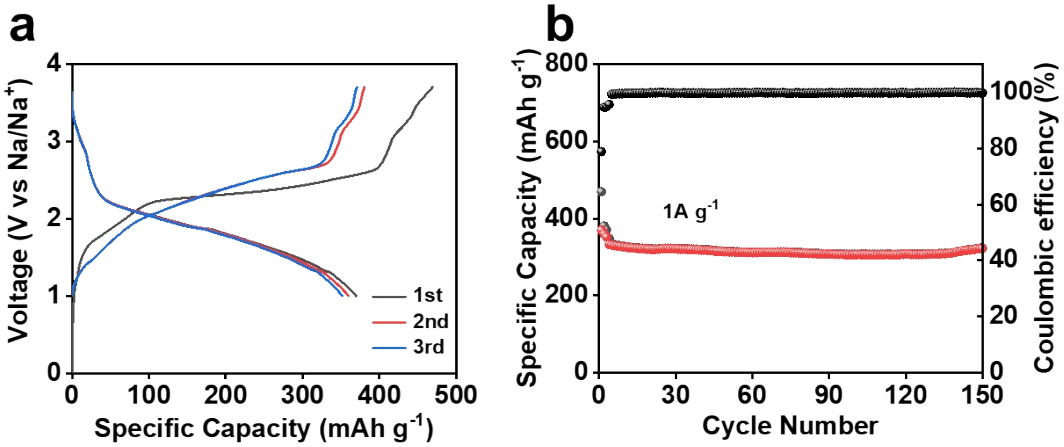

Fig. S9 a) GCD profiles in the initial three cycles. b) Cycle performance at 1 A g^{-1} of the full cell in the voltage range of 1 ~ 3.7 V.

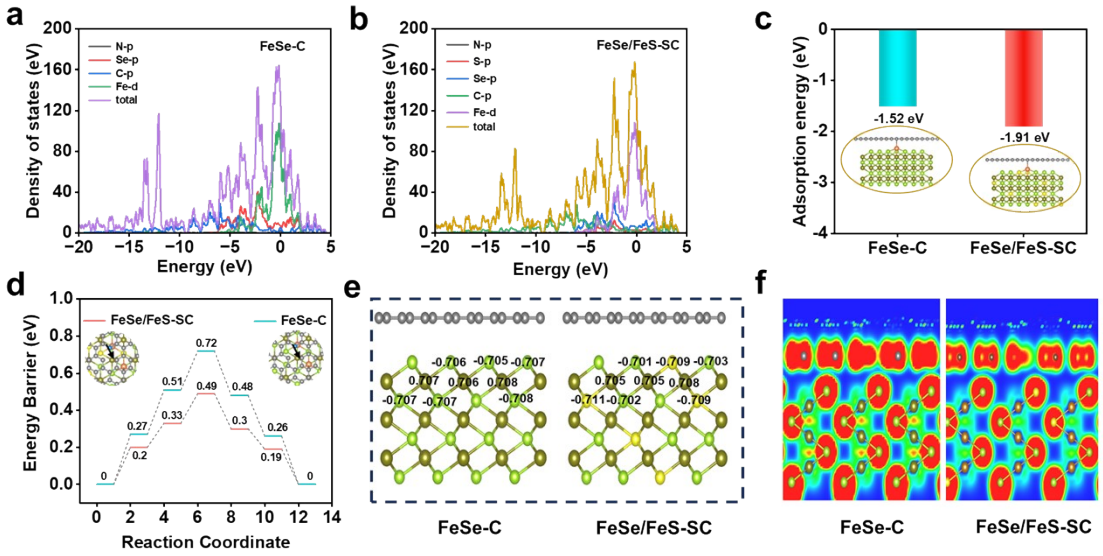

Figure S10 (a-b) Calculated DOS of FeSe-C and FeSe/FeS-SC. (c) Na adsorption energies. (d) Energy barrier profiles along the Na diffusion pathway and the corresponding top views of diffusion pathways. (e) Atomic charge distribution of FeSe-C and FeSe/FeS-SC. (f) Electron localization function (ELF) of FeSe-C and FeSe/FeS-SC.